Electrochemical Properties and Relaxation Times of the Hematite/Water Interface

ARTICLE *in* LANGMUIR · JULY 2014

Impact Factor: 4.46 · DOI: 10.1021/la501669a · Source: PubMed

2 AUTHORS:

Kenichi Shimizu
University of Oxford
17 PUBLICATIONS **311** CITATIONS
SEE PROFILE

Jean-François Boily
Umeå University
87 PUBLICATIONS **1,648** CITATIONS
SEE PROFILE

Langmuir

Article

pubs.acs.org/Langmuir

Electrochemical Properties and Relaxation Times of the Hematite/Water Interface

Kenichi Shimizu and Jean-François Boily*

Department of Chemistry, Umeå University, Umeå SE-901 87, Sweden

Supporting Information

ABSTRACT: Electric double layer properties and protonation rates at the surface of a mechanically and chemically polished (001) surface of hematite (α-Fe_2O_3) contacted with aqueous solutions of NaCl were extracted by electrochemical impedance spectroscopy (EIS). Effects of pH (4−12) and ionic strength (10−1000 mM) on the EIS response of the electrode were predicted using an electrical equivalent circuit model accounting for hematite bulk and interfacial processes. These efforts generated diffuse layer as well as compact layer capacitances and resistance values pertaining to interfacial processes. Diffuse layer capacitance values lie in the 0.5−0.6 μF cm^{-2} region and are about 1.5 times smaller than those obtained on a roughened hematite surface. Compact layer capacitances are strongly pH dependent as they pertain to the transfer of ions (charge carriers) from the diffuse layer onto surface (hydr)oxo groups. These values, alongside those of resistance adsorption, pointed a 50% decrease in proton adsorption/desorption resistance under acidic and alkaline conditions relative to that of the point of zero charge (pH 8−9). Increasing ionic strength generally induces larger diffuse layer capacitances, larger adsorption capacitances, and lower resistance values. Such a response is in line with the concept for thinner electric double layers and facilitated proton adsorption reactions by solutions of high ionic strengths. Relaxation times pertaining to the transfer of charge carriers across the compact plane induced by the EIS experiments lie in the 0.7−4.2 s range and become larger under acidic conditions. Decreases in site availability and increases in electrostatic repulsion are two possible contributing factors impeding reaction rates below the point of zero charge. Collectively, these finding are underpinning important relationships between classical views on mineral surface complexation reactions and electrochemical views of semiconductor/water interfaces.

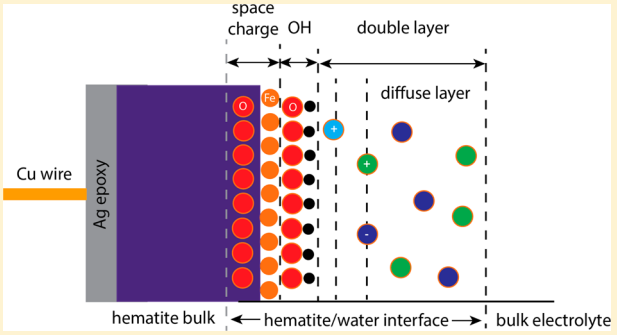

1. INTRODUCTION

Mineral/water interface (bio)(geo)chemistry plays a central role in a variety of natural and technological processes.[1−3] Reactions taking place at hematite (α-Fe_2O_3) surfaces are of particular interest for these two areas considering the widespread occurrence and reactivity of this phase. As hematite often occurs as an n-type semiconductor—and with a band gap of 2.1 eV—interfacial electrochemical processes can often be coupled to electron transport to the mineral bulk.[4,5] Such reactions can facilitate, for instance, photoassisted water splitting reactions in technological and coupled microbial−mineral electron transfer processes in biogeochemical settings.[6] A fundamental knowledge of hematite/water interfacial chemistry is thereby crucial for predicting its contributions in variety of important processes.

Experimental studies dedicated to hematite/water interfacial chemistry have involved slurries of nano- to microsized particles[7−11] as well as single crystal/whole body particles.[12−22] Work along the latter front has involved crystal truncation rod,[17−19] X-ray reflectivity,[15,20] tomography,[23−25] and atomic and scanning tunneling microscopy[21] methods. These efforts have led to compelling descriptions of hematite surface structure, composition, and topography exposed to a variety of aqueous solution compositions. Electrochemical techniques applied to this semiconductive material have also included direct open circuit potential (E_{oc}) measurement,[26−29] cyclic voltammetry (CV),[10,30] and electrochemical impedance spectroscopy (EIS).[30,31] These approaches have experienced increased interest as possibly catalyzed by evidence[4] underpinning a linked reactivity between interfacial and bulk processes. Single crystal electrode studies have, in this respect, been instrumental in identifying effects of crystal plane orientation on the development of electric potentials resulting from the adsorption of potential determining ions (pdi).[32] Recent work[33] also presented E_{oc} values for annealed hematite surfaces of various crystallographic orientations. CV studies have, in the same token, provided complementary information in related contexts such as resolving the redox stabilities of hematite surfaces.

An even more explicit extraction of interfacial properties (e.g., capacitance and resistance) can be effectively be carried out by EIS.[30,34−37] EIS measures the opposition of the flow of

Received: April 29, 2014
Revised: July 13, 2014
Published: July 15, 2014

   dx.doi.org/10.1021/la501669a | Langmuir 2014, 30, 9591−9598

electrons occurring in an electrode subjected to an externally applied an alternating voltage of various frequencies. A schematic representation of an equivalent electric circuit representing a hematite electrode contacted with an aqueous solution is shown in Figure 1. The ratio of the Fourier

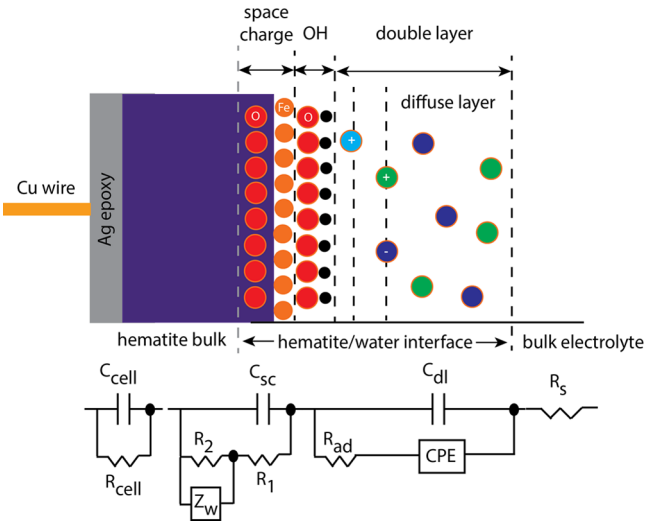

Figure 1. Schematic representation of the hematite/water interface in the electrode setup (top) and the equivalent circuit model used for EIS modeling (bottom). The equivalent circuit model consists of two components: the solid phase and the aqueous phase. The solution side of the interface is represented by the following circuit components: solution resistance (R_s), a diffuse layer capacitance (C_{dl}), and a CPE as well as a resistance (R_{ad}) for charge-carrier transfer from the diffuse to the compact layer. The solid-phase terms include the capacitance of the space charging layer (C_{sc}), the ohmic resistance (R_1), and the charge transport (R_2) and charge diffusion (Z_w).

transforms of the applied voltage and measured current is used in expressing these data, typically in a complex plane (Nyquist) plot.[36] These data are then fitted using equivalent electrical circuit models consisting of a combination of resistors and capacitors representing frequency-resolved processes (Figure 1). By scanning impedance over a range of frequencies—typically 0.1 Hz to 100 kHz—models can be used to distinguish between relatively fast electrochemical processes involving electron transport in the hematite bulk from slower electrostatic reactions involving the transfer of ions through compact and diffuse layers. In addition, EIS measurements on single whole body electrodes, rather than nanosized particles deposited on electrode surfaces,[10,38−41] offer the added benefit of resolving such processes on crystallographically oriented surfaces.

This study builds upon previous EIS work from our group[30] focused on electrodes cut from a single hematite specimen. In this work we use a new experimental setup (Figure 2 and Figure S1 of Supporting Information) that enables fresh aqueous solutions to be reacted with the electrode surface with the aim at resolving electric double layer properties of the hematite basal (001) plane/water interface. Although the basal plane is ideally charge neutral and amphoterically silent and terminated by doubly coordinated hydroxo groups, alternative and/or coexisting sites include those of the type $(OH)_3$−Fe−H_3O_3−R (oxygen-terminated) and $(OH)_3$−Fe−Fe−R (iron adatoms),[42] especially that the imperfect surface considered for this work was not annealed but mechanically and chemically polished. The EIS response of this system is then used to

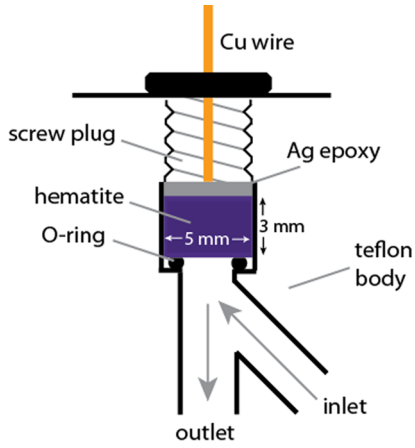

Figure 2. Portion of experimental setup for open circuit and EIS measurements. A 5 mm × 5 mm × 3 mm hematite is squeezed against a 3 mm wide O-ring into a Teflon cell using a hollow polyethylene screw. The backside of the hematite sample is electrically connected to a Cu wire using Ag epoxy. The aqueous solution is pumped through the cell to and from an airtight titration vessel containing a Ag/AgCl electrode as a Pt mesh which, alongside the Cu wire, are connected to a potentiostat. A pH electrode is, in turn, connected to an electrically isolated pH meter.

extract resistance (R) and capacitance (C) values of solution, interfacial, and hematite bulk processes. Some of these results are also contrasted to those obtained on a rougher electrode surface presented in a previous study from our group.[30] Parameters corresponding to RC-like circuit components of the near hematite/water interface were also used to extract relaxation time values of charge carrier transfer across the compact plane. These values shed further insight into the driving mechanisms controlling hematite/water interface reactivity of this geochemically and technologically important system.

2. EXPERIMENTAL SECTION

2.1. Electrode Preparation and Characterization. A 5 mm × 5 mm × 3 mm natural hematite specimen was obtained from an unspecified location by SurfaceNet (Rheine, Germany). It was cut and physically and chemically polished along the ⟨001⟩ direction. The sample was sonicated for 1 min periods first in acetone, then in ethanol, and finally in water. After thoroughly rinsing the crystal surface with ultrapure water, the specimen was dried under a stream of dry N_2(g).

Surface topography was imaged using an atomic force microscope (AFM; PICO PLUS, Agilent). Imaging was operated under tapping mode using an 100 μm scanner with acoustically driven cantilevers operating at a resonance frequency in the 320−370 kHz range. Scanning resolution was 512 × 512 pixels. The resulting AFM images (Figure 3) reveal a generally flat surface with topographical variations of the order of <10 Å, while faint trenches could be of natural cause as we cannot eliminate possible contributions from mechanical polishing alone. The surface is therefore not a true crystallographic representation of the (001) plane, although it should be stated that the bulk is highly oriented along this plane.

The composition of the electrode surface was determined by X-ray photoelectron spectroscopy (XPS). The spectra were recorded with a Kratos Axis Ultra electron spectrometer equipped with a delay line detector. A monochromated Al Kα source operated at 150 W, a hybrid lens system with a magnetic lens, providing an analysis area of 0.3 mm × 0.7 mm, and a charge neutralizer were used for the measurements. The resulting spectrum contains the characteristic Fe $2p_{3/2}$ and O 1s lines of hematite (Figure S2), yet no detectable impurities other than adventitious carbon moieties, i.e., carbon-based contaminants from the

dx.doi.org/10.1021/la501669a | Langmuir 2014, 30, 9591−9598

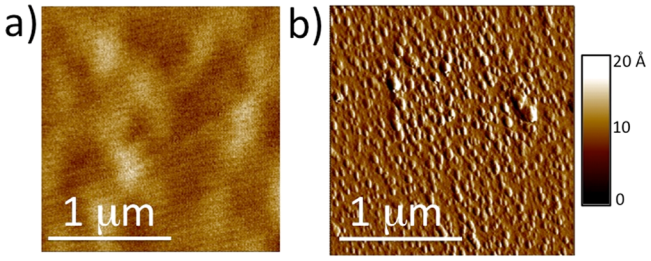

Figure 3. AFM images of the electrode surface before (a) and after (b) EIS experiments. Images are flattened using the second-order polynomial leveling in order to eliminate the height of the background caused by the tilted sample surface. This treatment is essential for observation of surface topology, as the heights associated with nanostructures are much smaller than that of the background.[55]

atmosphere, are found.[43] We should however stress that because this sample is of natural origin and that is electrically conductive (10−16 kΩ) its bulk is expected to contain some levels of dopants at levels below the limit of detection of the XPS (0.02 atomic %) at the top ∼10 nm surface (cf. Table 1 of ref 44). Using the equation $1/\rho = \mu Nq$ (where ρ is resistance in Ω·cm, μ = 200 $cm^2\ V^{-1}\ s^{-1}$ is our chosen charge mobility of the hematite bulk, N is dopant concentration in cm^{-3}, and $q = 1.6022 \times 10^{-19}$ C), we evaluate the dopant densities to lie in the $2.0-3.1 \times 10^{12}$ cm^{-3} (0.10−0.15 nmol/mol hematite) range.

2.2. Electrochemical Measurements. Electrochemical measurements were carried out using the conventional three-electrode cell configuration consisting of the working hematite single crystal electrode, an Ag/AgCl reference electrode (3 M KCl, Mettler Toledo Inlab Reference), and a platinum mesh auxiliary electrode, as shown in Figure S1. The working electrode was constructed by electrically connecting the underside of the hematite specimen with a Cu wire using Ag epoxy. The electrode was then mounted against a Teflon O-ring in a single Teflon body (Figure 2 and Figure S1), exposing a circular area with a 3 mm diameter of its polished oriented surface to aqueous solutions, as well as excluding light from the system. In contrast to traditional setups, where all electrodes are in close contact with one another, the working electrode was separated by a narrow capillary tube from the reference and counter electrodes. The potential drop caused by the ∼60 cm separation between the electrodes is 3.5 mV at 10 mM, 1.6 mV at 100 mM and 0.2 mV at 1000 mM NaCl.

Aqueous solutions were pumped through the cell at a rate of ∼35 mL/min through a 3 × 3 mm capillary contacted the hematite surface at a ∼45° angle and left the surface at a right angle. This configuration ensured proper mixing, minimized accumulation of air bubbles at the hematite/water interface, and flushed any dissolved species arising from the hematite surface, if present. Aqueous solutions of 10, 100, and 1000 mM NaCl were adjusted for pH in an external titration vessel under an atmosphere of N_2(g). Experiments were started in thoroughly degassed solutions of pH 5.8−6.8 and then titrated to pH 11−12 with NaOH and then back to pH 4−5 with HCl. All titrants were at the same ionic strength and ionic composition as the background electrolyte. After each titrant addition, solutions were circulated through the Teflon cell (Figure S2) using a mechanical pump until the pH electrode (Mettler Toledo Inlab Routine-L) reached stable readings. E_{oc} and pH values were monitored for at least 40 min at each solution composition considered in this work, after which time the former values attained a drift of less than 1−2 mV h^{-1}. An EIS experiment was thereafter carried out by applying a bias potential corresponding to experimental E_{oc} value and changing the frequency from 100 kHz to 0.1 Hz using a working amplitude of 25 mV. EIS data were fitted to the equivalent circuit model of Figure 1 using the program ZView (v. 3.1, Scribner Associates Inc.). A variety of models were tested during the course of these procedures. The circuit of Figure 1 is a slight modification of the one used in our previous EIS study[30] and was chosen based on its ability to reproduce the data, as evaluated by a statistical analysis used to objectively determine the optimal number of significant adjustable parameters (cf. section 3.2.1).

Finally, CV measurements were carried out using the same experimental setup by sweeping the 0−1 $V_{Ag/AgCl}$ range at scan rates of 10, 20, 50, 100, and 200 mV/s. These measurements were performed at pH 4 and 10 after all EIS data were collected. All EIS and CV measurements were conducted using Princeton Applied Research 273A potentiostat/galvanostat with a model 1250A frequency response analyzer (Solartron Analytical).

3. RESULTS AND DISCUSSION

3.1. Electrode Functionality and Potential Development. E_{oc} values (Figure 4) were obtained from thoroughly

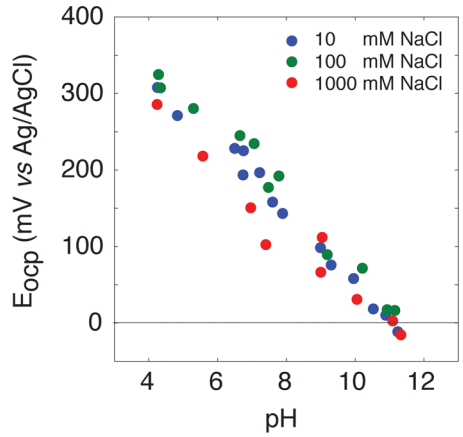

Figure 4. Open circuit potential of the hematite electrode contacted with 10, 100, and 1000 mM NaCl at 25 °C.

equilibrated systems between each change in solution composition and EIS experiments. In all cases were experiments reversible, and with drifts in E_{oc} of less than 1−2 mV h^{-1}. The systems under study lack any of the hysteresis features reported in studies in related systems[27,32,44,45] and therefore do not provide any evidence for a recently proposed[33] charge trapping/shielding mechanism for the sample type under study. All values were moreover sub-Nernstian in behavior, with ionic strength independent slopes of −46 mV/pH (10 mM), −44 mV/pH (100 mM), and −39 mV/pH (1000 mM). In all cases are proton-active (hydr)oxo surface sites responsible for the pH-dependent potential development. Those of the basal (001) plane likely outcrop at imperfections (e.g., roughness and adatoms) and override intrinsic contributions from the relatively proton inactive μ-OH groups of the idealized termination. This concept is supported further by AFM imaging of the electrode surface prior experimentation (Figure 3), showing topographical variations of the order of 5−7 Å. These imperfections are, on the other hand, substantially smaller than those considered in a previous study from our group where an electrode surface was purposefully roughened.[30] Results of that study will be recalled in the next sections to emphasize differences between those roughened surface and the one considered in this work. We also note that AFM images of the electrode after the experiments reveal a collection of mound-like formations of about 50 nm in diameter. These features could have resulted from dissolution and nanoparticle growth and/or deposition. While this should not have occurred under the conditions of the EIS experiments, a possible redox-driven growth akin to the pyramidal-like features discussed by Yanina and Rosso[4] could have occurred during the ensuing CV experiments. The precise nature of these features is currently under further investigation.

dx.doi.org/10.1021/la501669a | Langmuir 2014, 30, 9591−9598

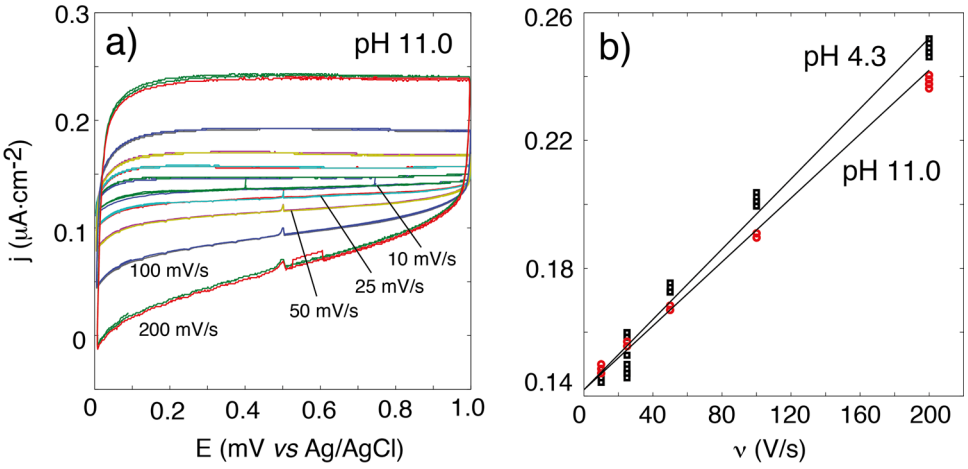

Figure 5. Cyclic voltammetry of the hematite electrode at pH 11 in 100 mM NaCl (a) and steady-state current density (j) as a function of the sweep rate (υ) from the cyclic voltammograms at a constant potential of 0.4 mV (b).

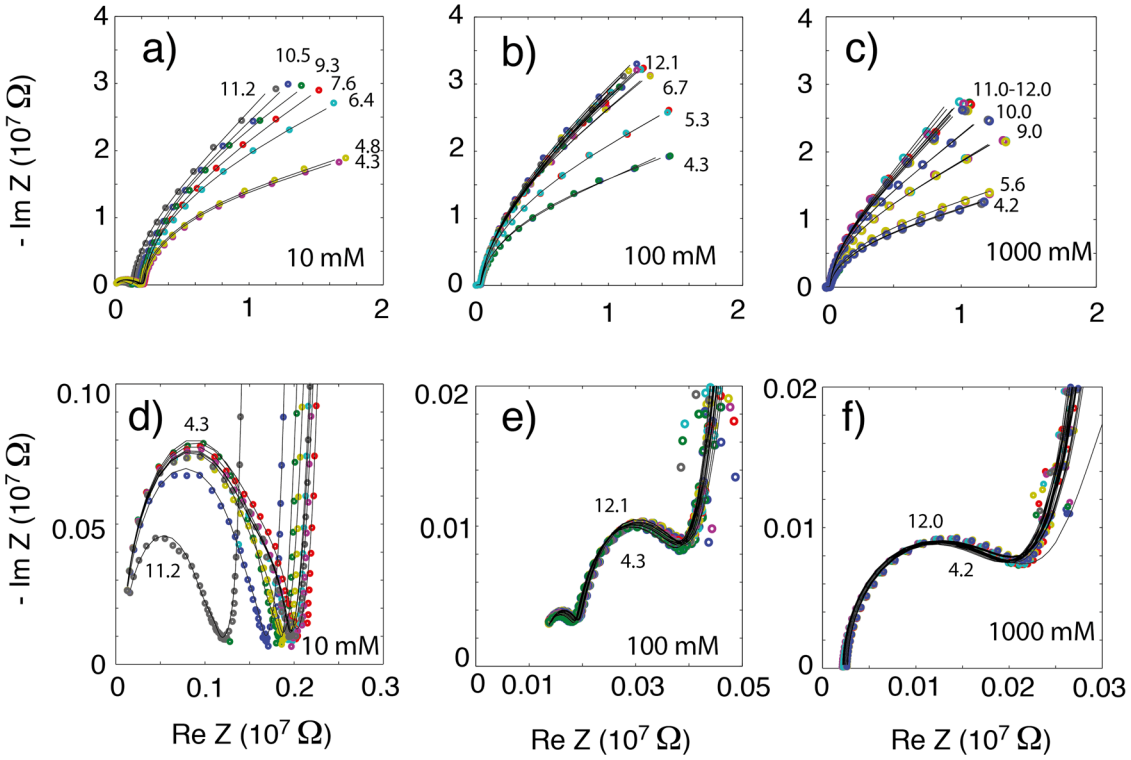

Figure 6. Nyquist plot showing complex plane plots (Re = real; Im = imaginary) for the hematite electrode in 10 (a, d), 100 (b, e) and 1000 mM (c, f) NaCl as a function of pH. Full lines show fits obtained with the equivalent circuit model of Figure 1, using eq 1. Modeling parameters are reported in Table 1 of ref 44. Lower and upper pH values are also indicated in all plots.

CV (Figure 5), which was performed after all EIS measurements, confirmed further the functionality of the electrode. The details of these features are highly comparable to those presented in an earlier study.[30] Steady-state current densities (j) obtained in the flat region of the voltammograms and at sweep rates (υ) in the 10−200 mV s^{-1} range were used to extract the interfacial capacitance (C_{int}) of the system, with the relationship $j = \upsilon C_{int}$.[46] This capacitance, in contrast to those extracted by EIS, pertains to the entire region encompassing both compact and diffuse layers as well as contributions from space charge layer of the hematite bulk surface (Figure 1). The results (Figure 5) was largely linear over the entire range of sweep rates, with C_{int} = 0.55 μF cm^{-2} at pH 4.3 and C_{int} = 0.50 μF cm^{-2} at pH 11.0. These values are considerably lower than the 2.0−3.1 μF cm^{-2} values obtained by the same method on the rougher electrode surface considered in our previous study[30] and will be extracted more explicitly by EIS.

3.2. EIS of the Hematite/Water Interface. All EIS data (Figure 6) consist of two predominant frequency-resolved regions. The 10 kHz−200 Hz region (Figure 6d−f) pertains to processes taking place in the hematite bulk and is shown in the 0−0.25 × 10^7 Ω (real Z) region of the Nyquist plots. The region below 200 Hz pertains to, on the other hand, interfacial and aqueous solution processes and is shown in the region above 0.25 × 10^7 Ω (real Z).

dx.doi.org/10.1021/la501669a | Langmuir 2014, 30, 9591−9598

The high frequency 200 Hz−100 kHz region is characterized by semicircles in the Nyquist plot that can be accounted for using a simple *RC* parallel circuit. While not considerably affected by the changes in pH at 100 and 1000 mM NaCl, the cell resistance is strongly affected at 10 mM. In this latter case, the semicircle is merged with the midfrequency impedance response of bulk hematite. As the product of *R* and *C* varies with ionic strength, this result may have arisen from the slower relaxation time of the electrolyte ions. This effect is not normally observed for this frequency range and ionic strengths when electrodes are situated closely in the electrochemical cell, as was notably seen in our previous study[30] where we used a conventional three-electrode setup dipped into a single reaction vessel. In this study, the narrow and long capillary tube of our cell separated the crystal working electrode from the reference and counter electrode and induced this specific spectral feature. The equivalent circuit originally proposed in our previous work[30] was therefore modified to fit this region.

The region above 0.25×10^7 Ω (real *Z*) (below 200 Hz) is strongly affected by variations in pH as these arises from interfacial and aqueous solution processes (Figure 1). These data show that proton adsorption reactions strongly attenuate imaginary *Z* values of the Nyquist plots. Phenomenological explanations to these variations, as well as potential effects of ionic strength, will be extracted by modeling these data using a variant of equivalent circuit model of Shimizu et al.,[30] as will be discussed in the following sections. The pH and ionic strength dependence of the fitting parameters of this circuit will then be discussed in the final section of this paper.

3.2.1. Equivalent Circuit. Extraction of double layer resistance and capacitance values of the hematite/water interface was carried out using the equivalent circuit of Figure 1, representing the frequency-dependent impedance data. Slight variations from this circuit model were previously applied on a similar setup for hematite and are originally developed for a TiO_2 single-body electrode by Bondarenko and Ragoisha.[47] As discussed in our previous work,[30] this model represents the impedance response of the experimental setup by (i) the hematite bulk at 10 kHz−200 Hz, (ii) the interfacial region comprising a compact layer and a diffuse layer at <10 Hz, and (iii) the bulk electrolyte region (i.e., cell resistance).

Contributions from the hematite bulk (10000−200 Hz) are represented by (i) ohmic resistance ($Z_1 = R_1$), (ii) space charge capacitance of the depletion layer ($Z_{sc} = (j\omega C_{sc})^{-1}$), where ω is the angular frequency, and (iii) electron−hole recombination, namely charge trap and diffusion, which are here treated as a constant phase element (CPE; $Z_w = T^{-1}(j\omega)^{-0.5}$) and transport ($Z_2 = R_2$). The CPE component accounts for the slope of the low-frequency region and where the associated φ term was optimized to denote the nonideal behavior of electron flow. The resistance term Z_w accounts for processes including electron−hole recombination, charge diffusing, and charge trapping at the conduction bands as well as charge leakage due to structural defects and/or impurities. This term was also included in the recent study of Klahr et al.[10] on hematite photoelectrodes. The C_{cell} and R_{cell} parameters represent the cell constant arising from our new cell design, which, in contrast to our previous study, now consists of capillaries separating our working electrode from the reference. As described in the previous section, the impedance response represented by C_{cell} and R_{cell} pertains to the dielectric relaxation of electrolytes in the bulk solution. Hence, this effect is not specifically related to property of the working electrode. These parameters should thereby change as the solution conductivity changes, yet they are very small if not negligible for the 1000 mM solutions. Taking into account the serial and parallel combinations of these circuit elements, the equation representing the bulk contributions to the EIS data becomes

$$Z_{tot} = \frac{1}{j\omega C_{sc} + \frac{1}{R_1 + \frac{R_2}{(j\omega)^{0.5} T_w R_2 + 1}}} + \frac{1}{j\omega C_{sc} + \frac{1}{R_{rc,1} + \frac{1}{(i\omega)^{0.5} T_{sc} + \frac{1}{R_{rc,2}}}}} + \frac{1}{j\omega C_{Cell} + \frac{1}{R_{Cell}}} \quad (1)$$

In contrast to bulk processes, interfacial processes are manifested at intermediate to low frequencies (<10 Hz). Double layer charging and surface (de)protonation reactions are the two predominant interfacial processes, and their equivalent circuit components occur in parallel. The double layer charging arises from the response of free electrolyte ions and can hence be addressed by the capacitance term $Z_{dl} = (j\omega C_{dl})^{-1}$. The (de)protonation process is affected by surface properties including site geometry and density. A constant phase element (CPE), $Z_{CPE} = T_{ad}^{-1}(j\omega)^{-\varphi}$, is in this case used to account for ionic adsorption. Moreover, unlike the diffuse layer process, the compact layer process involves formation/dissociation of O−H bonds (428 kJ/mol),[48] hence the inclusion of the adsorption resistance ($Z_{ad} = R_{ad}$) term in our equivalent circuit. The terms of the compact plane pertain to the capacitive and resistive contributions of the transfer of potential determining ion (H^+, OH^-). The CPE was, in this case, required for the capacitance term to fit the data. Its associated φ term was optimized to denote the nonideal behavior of compact plane, one that could be attributed to imperfections including nonuniform current distribution and surface roughness. The equation representing interfacial and solution contributions to the EIS data is therefore

$$Z = \frac{1}{j\omega C_{dl} + \frac{1}{R_{as} + \frac{1}{(j\omega)^{\phi} T_{ad}}}} \quad (2)$$

as it was in our previous work.[30] This equation, in combination with eq 1, can now be used to reproduce all EIS data of Figure 6 using the parameters shown in Figure 7. Note that CPE φ values (not shown) lie in the 0.50−0.83 range.

3.2.2. Equivalent Circuit Parameters. Salient circuit parameters pertaining to the hematite bulk (Figure S3) are largely pH independent and lie outside the scope of this study. Those of the interface are, in contrast, more relevant to the aims of this study and can be described as follows.

Double layer capacitance values (Figure 7) are all predominantly the C_{dl} = 0.5−0.6 μF cm^{-2} range and thus highly comparable to those extracted by CV (section 3.1). These values are about 1.5 times lower than those derived from our earlier study on a hematite electrode with an undefined, rougher, surface. These lower values thereby correlate with a decreased ability for the more pristine (001) plane at accumulating surface charge. C_{dl} values are lowest in the 6.5−9.0 range (Figure 7a), as also seen in our earlier study where a clearer minimum was observed near the point of zero charge. We also note that values are larger in the 1000 mM system, consistent with the concept that mineral surfaces contacted with concentrated electrolyte solutions are of larger capacitance

dx.doi.org/10.1021/la501669a | *Langmuir* 2014, 30, 9591−9598

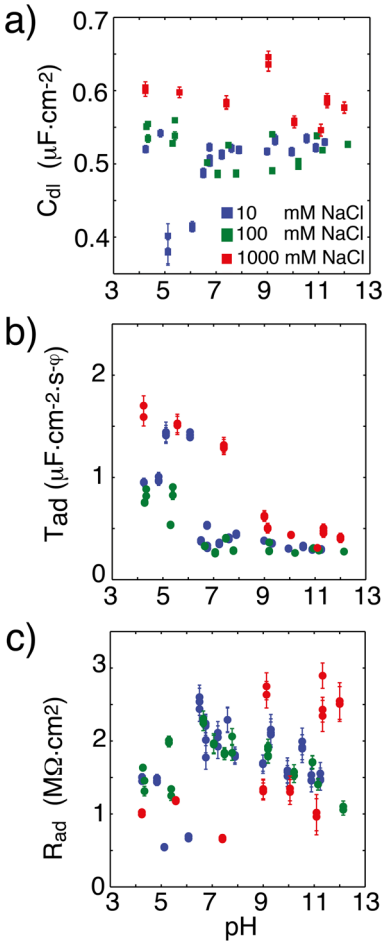

Figure 7. pH and ionic strength dependence of capacitance and resistance components of the hematite/water interface: (a) diffuse layer capacitance (C_{dl}), (b) CPE capacitance (T_{ad}), and (c) compact layer resistance (R_{ad}). Note that units of T_{ad} are μF cm^{-2} s$^{-\varphi}$ as $\varphi < 1$ as the CPE is an imperfect capacitor. All results are corrected for the geometrical surface area of the electrode (0.071 cm^2).

values. No clear distinction could be made between the 10 and 100 mM data.

Values of the T_{ad} lie in the 0.2−2.0 μF cm^{-2} s$^{-\varphi}$ range and are therefore larger than those of C_{dl}. T_{ad} values are, furthermore, more than 15 times lower than on a previously studied[30] roughened surface. This may also point to lower ionic loadings achieved at the electrode surface and denote a thicker molecular capacitor of relatively smaller charge storage capacity, such as characteristic of compact layers. Furthermore, as in the case of C_{dl}, T_{ad} is larger in the 1000 mM system below pH 9 as well as in the 10 and 100 mM systems below pH 7. This, in tandem with the aforementioned evidence for the development of surface charge at low pH, could potentially be explained by the accumulation of chloride ions at the hematite/water interface.

Finally, R_{ad} values (Figure 7c) add further information on the resistance associated with proton adsorption/desorption reactions. Although some scatter is apparent in the 1000 mM data, the lower ionic strengths reveal lower R_{ad} values that are up to 50% lower at low and high pH than at the point of zero charge. These regions of smaller resistance are attributable to faster reaction kinetics for surface (de)protonation reactions. These may, moreover be facilitated favorable electrostatic conditions induced by counterion (e.g., Cl^-, Na^+) adsorption.

3.2.3. Relaxation Time of Interfacial Charge Carriers. As EIS is a technique that perturbs interfacial equilibrium states by applying ac voltages to the system, it provides here a means to extract relaxation time (τ) of specific processes. Those pertaining to the transfer of ions (charge carriers) from the diffuse layer to hydroxyls of the hematite surface can be derived from our values of T_{ad} and R_{ad}. This can be effectively obtained using the Brug[49] conversion of CPE to capacitance:

$$C_{ad} = T_{ad}^{1/\varphi} R_{ad}^{(1-\varphi)/\varphi} \quad (3)$$

Then, we can extract relaxation time with

$$\tau = C_{ad} R_{ad} \quad (4)$$

Our resulting values (Figure 8) range from 0.7 s under alkaline conditions to 4.2 s under acidic conditions. They are also

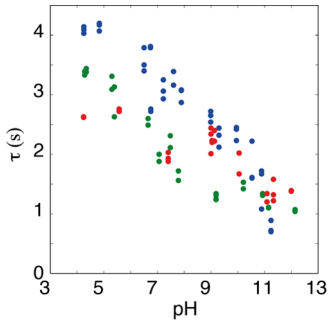

Figure 8. EIS parameters-derived relaxation times (eq 4) of the hematite/water interface. Legend for colored symbols are the same as in Figure 7.

comparable to proton desorption values obtained by pressure jump measurements in acidic suspensions of other iron oxide colloids.[26,50] NMR-derived lifetimes of hydroxyl protons in the Al_{13} ε-keggin polyoxocation are, on the other hand, in the microseconds to milliseconds time scale, although it should be stressed that the different nature of the experiment may have caused this as well.[51] The pH dependency of our values is more similar to those of C_{ad} (eq 3) and T_{ad} (Figure 7), and considerably less with R_{ad}. The data suggests that protonated sites are less quickly re-equilibrated under acidic media under the ±25 mV ac current of the EIS experiment. The compounded effects of increased site occupancy and repulsive electrostatic forces acting upon interfacial protons/hydronium ions should be responsible for these results. This interpretation falls in line with the generally greater τ values at low ionic strengths, which could arise from greater electrostatic repulsion by the thicker diffuse layer generated under these conditions. In the same token, specific binding or exchange of ions with surface hydroxo/aquo groups, especially at low pH and high ionic strength, may contribute in shortening relaxation times. Taken collectively, these observations therefore pointing to important controls on relaxation times of charge carriers across the hematite/water interface by interfacial speciation and electric double layer properties.

4. CONCLUSIONS

The electrochemical impedance spectroscopic response of the oriented (001) plane of hematite contacted with aqueous solutions of NaCl is manifested in both high- and low-frequency regimes. Those of the high-frequency regime do not specifically arise from hematite bulk effects but rather to the

dx.doi.org/10.1021/la501669a | Langmuir 2014, 30, 9591−9598

configuration of the new cell under study. The separation of the working and reference electrodes induces ionic strength effects, especially at low salt concentration due to slower relaxation times for electrolyte ions. Those at low frequency pertain to, on the other hand, pH and ionic strength dependent interfacial processes.

The EIS response to pH and ionic strength is manifested by variations CPE capacitances (T_{ad}) and resistances (R_{ad}) pertaining to proton adsorption reactions. Adsorption resistance is least under acidic and alkaline conditions, yet more substantially attenuated at the largest ionic strength. Adsorption capacitance is, on the other hand, substantially increased at low pH and high ionic strength, as can potentially be understood by a thinning of the compact plane with adsorption. This latter concept is also retrieved in C_{dl} values, which are greater in 1000 mM NaCl. These values, just as those extracted by CV, are considerably smaller than a rougher electrode surface considered in a previous study.[30] They also exhibit a pH dependent trend with lowest values close to what could be perceived as a point of zero charge (~8−9) caused by a surface with amphoteric functional groups, again as seen in our previous work.[30] Relaxation times obtained from EIS-derived parameters are of the order 0.7−4.2 s and pertains to the ac-driven motion charge of carriers at the hematite/water interface. These values are larger under acidic conditions.

These efforts have now defined the basis of further work from our group where double layer properties of hematite surfaces contacted with aqueous solutions can be extracted more systematically for a variety of inorganic and organic solutes. This work, alongside other structural,[13,14,16,17,22,42,52] microscopic,[20,21] and molecular modeling studies,[53] will help resolve further the interfacial chemistry of this environmentally and technologically important mineral. Forthcoming studies along this front will consider effects of different (pristine and roughened) crystallographic terminations, solutes (e.g., NaCl, NH_4Cl, $NaHCO_3$), as well as light. Comparison of relaxation times in these different systems, and notably of predictions using methods such as activated adsorption desorption theory[26,54] supported by molecularly adequate thermodynamic adsorption models, will also open the way for representing a unified electrochemical−thermodynamical depiction of the semiconductive hematite/water interface.

■ ASSOCIATED CONTENT

Supporting Information

Figures S1−S3. This material is available free of charge via the Internet at http://pubs.acs.org.

■ AUTHOR INFORMATION

Corresponding Author

*E-mail jean-francois.boily@chem.umu.se; Ph +46 90 786 5270 (J.-F.B.).

Notes

The authors declare no competing financial interest.

■ ACKNOWLEDGMENTS

This work was supported by the Carl-Tyggers Foundation and by the Swedish Research Council (2012-2976).

■ REFERENCES

(1) Hochella, M., Jr.; Lower, S.; Maurice, P.; Penn., R. Nanominerals, mineral nanoparticles, and Earth systems. *Science* **2008**.

(2) Casey, W. H.; Rustad, J. R.; Spiccia, L. Minerals as molecules–use of aqueous oxide and hydroxide clusters to understand geochemical reactions. *Chemistry* **2009**, *15* (18), 4496−515.

(3) Paracchino, A.; Laporte, V.; Sivula, K.; Gratzel, M.; Thimsen, E. Highly active oxide photocathode for photoelectrochemical water reduction. *Nat. Mater.* **2011**, *10* (6), 456−461.

(4) Yanina, S.; Rosso, K. Linked reactivity at mineral-water interfaces through bulk crystal conduction. *Science* **2008**.

(5) Eggleston, C. M.; Shankle, A. J. A.; Moyer, A. J.; Cesar, I.; Gratzel, M. Anisotropic photocatalytic properties of hematite. *Aquat. Sci.* **2009**, *71* (2), 151−159.

(6) Meitl, L. A.; Eggleston, C. M.; Colberg, P. J. S.; Khare, N.; Reardon, C. L.; Shi, L. Electrochemical interaction of Shewanella oneidensis MR-1 and its outer membrane cytochromes OmcA and MtrC with hematite electrodes. *Geochim. Cosmochim. Acta* **2009**, *73* (18), 5292−5307.

(7) Boily, J. F.; Shchukarev, A. X-ray photoelectron spectroscopy of fast-frozen hematite colloids in aqueous solutions. 2. Tracing the relationship between surface charge and electrolyte adsorption. *J. Phys. Chem. C* **2010**, *114* (6), 2613−2616.

(8) Schudel, M.; Behrens, S. H.; Holthoff, H.; Kretzschmar, R.; Borkovec, M. Absolute aggregation rate constants of hematite particles in aqueous suspensions: A comparison of two different surface morphologies. *J. Colloid Interface Sci.* **1997**, *196* (2), 241−253.

(9) Shimizu, K.; Shchukarev, A.; Boily, J. F. X-ray photoelectron spectroscopy of fast-frozen hematite colloids in aqueous solutions. 3. Stabilization of ammonium species by surface (hydr)oxo groups. *J. Phys. Chem. C* **2011**, *115* (14), 6796−6801.

(10) Klahr, B.; Gimenez, S.; Fabregat-Santiago, F.; Bisquert, J.; Hamann, T. W. Photoelectrochemical and impedance spectroscopic investigation of water oxidation with "Co-Pi"-coated hematite electrodes. *J. Am. Chem. Soc.* **2012**, *134* (40), 16693−16700.

(11) Tilley, S. D.; Cornuz, M.; Sivula, K.; Gratzel, M. Light-induced water splitting with hematite: improved nanostructure and iridium oxide catalysis. *Angew. Chem., Int. Ed.* **2010**, *49* (36), 6405−6408.

(12) Yamamoto, S.; Kendelewicz, T.; Newberg, J. T.; Ketteler, G.; Starr, D. E.; Mysak, E. R.; Andersson, K. J.; Ogasawara, H.; Bluhm, H.; Salmeron, M.; Brown, G. E.; Nilsson, A. Water adsorption on alpha-Fe_2O_3(0001) at near ambient conditions. *J. Phys. Chem. C* **2010**, *114* (5), 2256−2266.

(13) Catalano, J. G.; Fenter, P.; Park, C. Water ordering and surface relaxations at the hematite (110)-water interface. *Geochim. Cosmochim. Acta* **2009**, *73* (8), 2242−2251.

(14) Catalano, J. G.; Fenter, P.; Park, C. Interfacial water structure on the (012) surface of hematite: Ordering and reactivity in comparison with corundum. *Geochim. Cosmochim. Acta* **2007**, *71* (22), 5313−5324.

(15) Catalano, J. G. Weak interfacial water ordering on isostructural hematite and corundum (001) surfaces. *Geochim. Cosmochim. Acta* **2011**, *75* (8), 2062−2071.

(16) Tanwar, K. S.; Catalano, J. G.; Petitto, S. C.; Ghose, S. K.; Eng, P. J.; Trainor, T. P. Hydrated alpha-Fe_2O_3(1(1)over-bar-02) surface structure: Role of surface preparation. *Surf. Sci.* **2007**, *601* (12), L59−L64.

(17) Tanwar, K. S.; Lo, C. S.; Eng, P. J.; Catalano, J. G.; Walko, D. A.; Brown, G. E.; Waychunas, G. A.; Chaka, A. M.; Trainor, T. Surface diffraction study of the hydrated hematite (1(1)over-bar-02) surface. *Surf. Sci.* **2007**, *601* (2), 460−474.

(18) Tanwar, K. S.; Petitto, S. C.; Ghose, S. K.; Eng, P. J.; Trainor, T. P. Structural study of Fe(II) adsorption on hematite(1(1)over-bar02. *Geochim. Cosmochim. Acta* **2008**, *72* (14), 3311−3325.

(19) Tanwar, K. S.; Petitto, S. C.; Ghose, S. K.; Eng, P. J.; Trainor, T. P. Fe(II) adsorption on hematite (0001). *Geochim. Cosmochim. Acta* **2009**, *73* (15), 4346−4365.

(20) Eggleston, C. M. The surface structure of alpha-Fe_2O_3 (001) by scanning tunneling microscopy: Implications for interfacial electron transfer reactions. *Am. Mineral.* **1999**, *84* (7-8), 1061−1070.

(21) Eggleston, C. M.; Stack, A. G.; Rosso, K. M.; Bice, A. M. Adatom Fe(III) on the hematite surface: Observation of a key reactive surface species. *Geochem. Trans.* **2004**, *5* (2), 33−40.

(22) Catalano, J. G.; Zhang, Z.; Park, C. Y.; Fenter, P.; Bedzyk, M. J. Bridging arsenate surface complexes on the hematite (012) surface. *Geochim. Cosmochim. Acta* **2007**, *71* (8), 1883−1897.
(23) Bachhav, M.; Danoix, F.; Hannoyer, B.; Bassat, J. M.; Danoix, R. Investigation of O-18 enriched hematite (alpha-Fe_2O_3) by laser assisted atom probe tomography. *Int. J. Mass Spectrom.* **2013**, *335*, 57−60.
(24) Echigo, T.; Monsegue, N.; Aruguete, D. M.; Murayama, M.; Hochella, M. F. Nanopores in hematite (alpha-Fe_2O_3) nanocrystals observed by electron tomography. *Am. Mineral.* **2013**, *98* (1), 154−162.
(25) Monsegue, N.; Jin, X.; Echigo, T.; Wang, G.; Murayama, M. Three-dimensional characterization of iron oxide (alpha-Fe_2O_3) nanoparticles: Application of a compressed sensing inspired reconstruction algorithm to electron tomography. *Microsc. Microanal.* **2012**, *18* (6), 1362−1367.
(26) Astumian, R. D.; Sasaki, M.; Yasunaga, T.; Schelly, Z. A. Proton adsorption-desorption kinetics on iron-oxides in aqueous suspensions, using the pressure-jump method. *J. Phys. Chem.* **1981**, *85* (25), 3832−3835.
(27) Preocanin, T.; Cop, A.; Kallay, N. Surface potential of hematite in aqueous electrolyte solution: Hysteresis and equilibration at the interface. *J. Colloid Interface Sci.* **2006**, *299* (2), 772−776.
(28) Kallay, N.; Preocanin, T. Measurement of the surface potential of individual crystal planes of hematite. *J. Colloid Interface Sci.* **2008**, *318* (2), 290−295.
(29) Boily, J. F.; Chatman, S.; Rosso, K. M. Inner-Helmholtz potential development at the hematite (alpha-Fe_2O_3) (001) surface. *Geochim. Cosmochim. Acta* **2011**, *75* (15), 4113−4124.
(30) Shimizu, K.; Lasia, A.; Boily, J. F. Electrochemical impedance study of the hematite/water interface. *Langmuir* **2012**, *28* (20), 7914−7920.
(31) Le Formal, F.; Pendlebury, S. R.; Cornuz, M.; Tilley, S. D.; Gratzel, M.; Durrant, J. R. Back electron-hole recombination in hematite photoanodes for water splitting. *J. Am. Chem. Soc.* **2014**, *136* (6), 2564−2574.
(32) Zarzycki, P.; Chatman, S.; Preocanin, T.; Rosso, K. M. Electrostatic potential of specific mineral faces. *Langmuir* **2011**, *27* (13), 7986−7990.
(33) Chatman, S.; Zarzycki, P.; Rosso, K. M. Surface potentials of (001), (012), (113) hematite (alpha-Fe_2O_3) crystal faces in aqueous solution. *Phys. Chem. Chem. Phys.* **2013**, *15* (33), 13911−13921.
(34) Gabrielli, C.; Grand, P. P.; Lasia, A.; Perrot, H. Investigation of hydrogen adsorption and absorption in palladium thin films - III. Impedance spectroscopy. *J. Electrochem. Soc.* **2004**, *151* (11), A1943−A1949.
(35) Hens, Z.; Gomes, W. P. On the electrochemical impedance of InP and GaAs electrodes in indifferent electrolyte. Part 2. Experimental study on the factors influencing the frequency dispersion. *Phys. Chem. Chem. Phys.* **1999**, *1* (15), 3617−3625.
(36) Lasia, A. *Electrochemical Impedance Spectroscopy and Its Applications*; Springer: Berlin, 2014; p 367.
(37) Sivula, K.; Le Formal, F.; Gratzel, M. Solar water splitting: Progress using hematite (alpha-Fe_2O_3) photoelectrodes. *ChemSusChem* **2011**, *4* (4), 432−449.
(38) Lopes, T.; Andrade, L.; Ribeiro, H. A.; Mendes, A. Characterization of photoelectrochemical cells for water splitting by electrochemical impedance spectroscopy. *Int. J. Hydrogen Energy* **2010**, *35* (20), 11601−11608.
(39) Bak, A.; Choi, W.; Park, H. Enhancing the photoelectrochemical performance of hematite (alpha-Fe_2O_3) electrodes by cadmium incorporation. *Appl. Catal., B* **2011**, *110*, 207−215.
(40) Bak, A.; Choi, W.; Park, H. Enhancing the photoelectrochemical performance of hematite (α-Fe_2O_3) electrodes by cadmium incorporation. *Appl. Catal., B* **2011**, *110*, 207−215.
(41) Karthik, K. R. G.; Mulmudi, H. K.; Jinesh, K. B.; Mathews, N.; Sow, C. H.; Huang, Y. Z.; Mhaisalkar, S. G. Charge transport in hierarchical alpha-Fe_2O_3 nanostructures. *Appl. Phys. Lett.* **2011**, *99* (13).
(42) Trainor, T. P.; Chaka, A. M.; Eng, P. J.; Newville, M.; Waychunas, G. A.; Catalano, J. G.; Brown, G. E. Structure and reactivity of the hydrated hematite (0001) surface. *Surf. Sci.* **2004**, *573* (2), 204−224.
(43) Smit, G. C. Evaluation of a simple correction for the hydrocarbon contamination layer in quantitative surface analysis by XPS. *J. Electron Spectrosc. Relat. Phenom.* **2005**, *148*, 21−28.
(44) Chatman, S.; Zarzycki, P.; Preoanin, T.; Rosso, K. M. Effect of surface site interactions on potentiometric titration of hematite (alpha-Fe_2O_3) crystal faces. *J. Colloid Interface Sci.* **2013**, *391*, 125−134.
(45) Zarzycki, P.; Rosso, K. M.; Chatman, S.; Preocanin, T.; Kallay, N.; Piasecki, W. Theory, experiment and computer simulation of the electrostatic potential at crystal/electrolyte interfaces. *Croat. Chem. Acta* **2010**, *83* (4), 457−474.
(46) Bard, A. J.; Faulkner, I. R. *Electrochemica Methods: Fundamentals and Applications.*; John Wiley & Sons: New York, 2000.
(47) Bondarenko, A.; Ragoisha, G. Variable Mott-Schottky plots acquisition by potentiodynamic electrochemical impedance spectroscopy. *J. Solid State Electrochem.* **2005**, *9* (12), 845−849.
(48) deB, D. B. Bond dissociation energies in simple molecules. *Nat. Stand. Ref. Ser. Natl. Bur. Stand.* **1970**, *176*, 275−295.
(49) Brug, G. J.; Vandeneeden, A. L. G.; Sluytersrehbach, M.; Sluyters, J. H. The analysis of electrode impedances complicated by the presence of a constant phase element. *J. Electroanal. Chem.* **1984**, *176* (1-2), 275−295.
(50) Piasecki, W.; Zarzycki, P.; Rudzinski, W. Relaxation time of proton adsorption from solution onto magnetite and anatase: Classical and new theoretical approach. *Croat. Chem. Acta* **2007**, *80* (3-4), 345−349.
(51) Houston, J. R.; Phillips, B. L.; Casey, W. H. Residence times for protons bound to three oxygen sites in the $AlO_4Al_{12}(OH)_{24}(H_2O)_{12}^{7+}$ polyoxocation. *Geochim. Cosmochim. Acta* **2006**, *70* (7), 1636−1643.
(52) Waychunas, G.; Trainor, T.; Eng, P.; Catalano, J.; Brown, G.; Davis, J.; Rogers, J.; Bargar, J. Surface complexation studied via combined grazing-incidence EXAFS and surface diffraction: arsenate an hematite (0001) and (10-12). *Anal. Bioanal. Chem.* **2005**, *383* (1), 12−27.
(53) Kerisit, S. Water structure at hematite−water interfaces. *Geochim. Cosmochim. Acta* **2011**, *75* (8), 2043−2061.
(54) Ashida, M.; Sasaki, M.; Kan, H.; Yasunaga, T.; Hachiya, K.; Inoue, T. Kinetics of proton adsorption-desorption at TiO_2-H_2O interface by means of pressure-jump technique. *J. Colloid Interface Sci.* **1978**, *67* (2), 219−225.
(55) Eaton, P.; West, P. *Atomic Force Microscopy*; Oxford University Press: Oxford, 2010.